On the control of the longitudinal-lateral vibration of a shaft-plate coupled system

Zhiyi Zhang[a] Yong Chen[a] Emiliano Rustighi[b] Hongxing Hua[a]

[a] State Key Laboratory of Mechanical System and Vibration, Shanghai Jiao Tong University, Shanghai, 200240, PRC
[b] Institute of Sound and Vibration Research, University of Southampton, Highfield, Southampton, SO17 1BJ, UK

Abstract: Modeling and control of the vibration of a shaft-plate coupled system are discussed. A simplified model of the system is established through synthesis of frequency response functions (FRFs) and verified with the finite element method, which exhibits the coupled vibration of the system induced by the longitudinal excitation at the free end of the shaft. Based on the analysis of dynamics, vibration control via longitudinal actuation on the shaft and active vibration cancellation are studied. The active control scheme is constructed on an adaptive feedback scenario and a mechanism of adaptation of the controller's gain, which is proposed to consider time-varying dynamics induced by the variation of stiffness of the axial spring. Simulation results have demonstrated that the control scheme enhanced with the proposed mechanism is effective in attenuating vibration of the system. Moreover, axial actuation on the shaft is able to cancel the effect of the longitudinal disturbance acting at the free end of the shaft and consequently reduces the internal forces as well as vibration in the plate. However, deviation of the actuation force from the shaft axis will deteriorate control of lateral vibration and sufficiently small deviation needs to be guaranteed.
Keywords: vibration control, adaptive feedback, time-varying system, longitudinal-lateral vibration, FRF synthesis

1 Introduction

Vibration of ship machinery may cause severe problems to ship safety, underwater environment as well as comfort of passengers. The application of passive isolators can alleviate the effect of machinery vibration to a large extent and well-isolated ship structures will have acceptable level of vibration. However, the propulsion system transmits vibration directly to ship structures and is usually one of the principal sources to structural vibration. Vibration control strategies associated with shafting systems have been studied for decades, but problems may still exist in new ship systems due to the complexity of shafting dynamics. Apart from vibration control techniques regarding bearing and shafting alignment, investigations have focused on reducing vibration of shafting systems and force transmission by inserting auxiliary systems to change dynamics of the original system. Mechanical facilities, such as passive/active vibration absorbers, elastic coupling and the resonance changer, have been used to control vibration induced by shafting systems [1-5].

Dynamics of shafting systems or shafting-structure coupled systems have been explored extensively in respect of vibration control. The early investigations considered only shafting systems and applied relatively simple models, such as models of finite degrees of freedom, to analyze dynamics of shafting systems with vibration control facilities. Such models are fundamental to the exhibition of problems in vibration control but not yet sufficient to describe interaction between the shafting system and foundation structures [5]. In recent years, investigations were conducted using more complicated models, such as FE/BE (finite element/boundary element) or FE models consisting of shafting systems and hull structures [6-7]. More valuable results about shafting-structure interaction and vibration control were obtained. However, it is not always convenient to use such numerical models for theoretical analysis of dynamics associated with vibration control. In contrast, delicate analytical models were also elaborated for analyzing shafting-structure coupled dynamics [8], but the disadvantage of analytical models is that they are not flexible enough to deal with structures of complicated boundary conditions. Hence, favorable methods are not only able to predict dynamics but also convenient to use in theoretical analysis, and hybrid models composed of numerical and analytical models are preferable in the exploration of vibration control of shafting-structure coupled systems. Except for theoretical investigations, there were also experimental researches on shafting dynamics and vibration control [9-10]. Experimental results have revealed that bearing parameters of the shafting system may vary in a wide range, which implies that the influence of time-varying characteristics needs to be considered in vibration control. It should be pointed out that active vibration control of time-varying shafting systems that are coupled with hull structures has not been investigated and the involved interaction is

not yet clear.

Active control methods, such as velocity feedback control and the optimal control, were applied to suppress vibrations in hull structures induced by the shafting system [5-6, 9]. In these investigations, however, the shafting system was treated as a time invariant system. In fact, when stiffness of the thrust bearing changes in a wide range, time-varying characteristics of the shafting system will be distinct and as a result should be considered in the construction of active control strategies. Moreover, uncertainties also exist in the variation of bearing stiffness, which unfortunately will cause difficulties to active vibration control because model identification for such a system is almost impossible. At the same time, disturbances on the shafting system are mainly composed of harmonics, which demands that control methods should have narrowband-disturbance-rejection capability. For LTI (linear time invariant) systems under harmonic excitation, adaptive methods and other model based methods, such as FxLMS (filtered-x least mean squares) and IMP (internal model principle), can be used to cancel disturbances [11-13], whereas for time-varying systems disturbance rejection is more complicated [14-16], especially in the circumstance that no model is available, which even rejects adaptive methods with online modeling. The promising method is SONIC (self-optimizing narrowband interference canceling), which does not need modeling and has been demonstrated effective for time-varying first/second-order systems [17-18] although it needs to be developed for higher order systems.

In this study, a simplified model is used to exhibit interaction between the shafting system and the support structures as well as the variation of dynamics in bearing stiffness. Actuation on the shaft is considered and a new adaptive scheme is proposed to deal with the time-varying system under harmonic excitation. This simplified dynamic model has abundant vibration modes and is accordingly sufficient for verification of the control scheme. The discussion is organized in six sections. Modeling of the simplified system is first presented in Section 2 and numerical simulation on the dynamics of this model is given in Section 3. Section 4 discusses the proposed adaptive scheme and Section 5 is the demonstration of the control scheme and active vibration suppression. Finally, conclusions are given in Section 6.

2 Modeling of the shaft-plate coupled system

Consider the shaft-plate coupled system shown in Fig.1, where the slender shaft is connected with the thin plate through two springs and one rigid joint. In this system, it is assumed that the plate is simply supported and the displacements of

Nomenclature:

ρ - Mass density
E - Modulus of elasticity
J - Area moment of inertia
A - Cross section area
L - Length of the shaft
h - Height of the rigid joint
k_s - Stiffness of the lateral spring
k_t - Stiffness of the longitudinal spring
δ - Thickness of the plate
D - Flexural stiffness of the plate
F - Disturbance force
F_a - Control force
l_x, l_z - Dimensions of the plate
l_a, l_b, l_s -Distances as illustrated in Fig.1

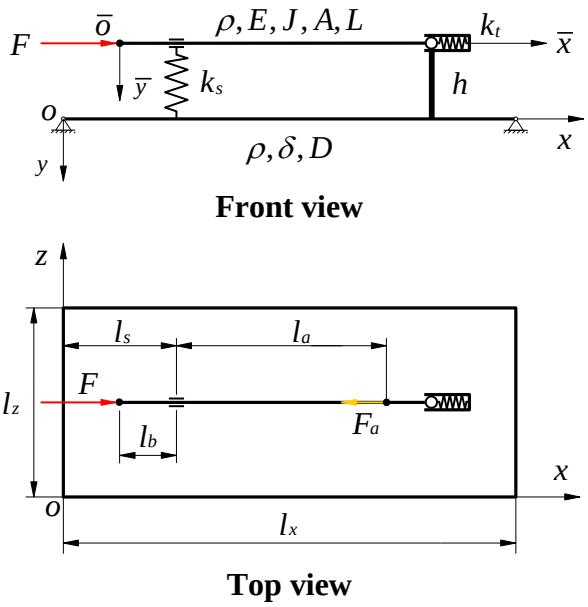

Fig.1 The shaft-plate coupled system

the shaft occur only in the $\bar{x}(x)$ and $\bar{y}(y)$ directions, moreover all deflections are sufficiently small so that the system behaves linearly. Under the excitation of the disturbance force F , as shown in the figure, the shaft-plate coupled system will vibrate and especially the shaft will vibrate in both the longitudinal and the lateral directions. Here, modeling of the vibration of this system is based on the synthesis of frequency response functions and accordingly FRFs associated with

the plate and the shaft need to be derived at first.

2.1 FRFs associated with the flexural vibration of the plate

Vibration equation of the plate can be described as [19]

$$\rho\delta\frac{\partial^2 w_p(x,z,t)}{\partial t^2}+D\nabla^4 w_p(x,z,t)=p(x,z,t) \tag{1}$$

where $D=\frac{1}{12(1-\nu^2)}E\delta^3$ is the flexural stiffness of the plate, δ is the thickness of the plate, ν the Poisson's ratio, E the modulus of elasticity, ρ the mass density, $w_p(x,z,t)$ the transverse displacement and $p(x,z,t)$ the load on the plate, $\nabla^4=\frac{\partial^4}{\partial x^4}+2\frac{\partial^4}{\partial x^2\partial z^2}+\frac{\partial^4}{\partial z^4}$.

Suppose $w_p(x,z,t)=W_p(x,z)e^{j\omega t}$, $p(x,z,t)=P(x,z)e^{j\omega t}$, $j=\sqrt{-1}$ and substitute them into Eq.(1), one has

$$D\nabla^4 W_p(x,z)-\rho\delta W_p(x,z)\omega^2=P(x,z) \tag{2}$$

Natural vibration modes of the plate satisfy the following characteristic equation, i.e.

$$D\nabla^4 W_{mn}(x,z)-\rho\delta\omega_{mn}^2 W_{mn}(x,z)=0,\ m\geq 1,\ n\geq 1 \tag{3}$$

where ω_{mn}, $W_{mn}(x,z)$ are natural frequencies and mode shapes, respectively. The amplitude of flexural displacements can be expressed in terms of these natural modes, i.e.

$$W_p(x,z)=\sum_{m,n=1}^{\infty}c_{mn}W_{mn}(x,z) \tag{4}$$

In Eqs.(3) and (4), ω_{mn}, $W_{mn}(x,z)$ are given by

$$\omega_{mn}=\sqrt{\frac{D}{\rho\delta}}\left[\left(\frac{m\pi}{l_x}\right)^2+\left(\frac{n\pi}{l_z}\right)^2\right],\ W_{mn}(x,z)=2\sin\frac{m\pi x}{l_x}\sin\frac{n\pi z}{l_z}.$$

Substituting Eq.(4) into Eq.(2) and taking into account orthogonality of mode shapes, one can arrive at

$$(K_{mn}-M_{mn}\omega^2)c_{mn}=P_{mn} \tag{5}$$

where $M_{mn}=\rho\delta l_x l_z$, $K_{mn}=M_{mn}\omega_{mn}^2$ and $P_{mn}=\int_0^{l_x}\int_0^{l_z}P(x,z)W_{mn}(x,z)dzdx$. Hence, combining Eqs.(4) and (5) leads to

$$W_p(x,z)=\sum_{m,n=1}^{\infty}\frac{W_{mn}(x,z)P_{mn}}{M_{mn}(\omega_{mn}^2-\omega^2)} \tag{6}$$

According to Eq.(6), when $P(x,z)=P\delta(x_1,z_1)$ is a point force, the FRF between the force and the displacement can be given as

$$H_{wp}(x,z,x_1,z_1)=\sum_{m,n=1}^{\infty}\frac{W_{mn}(x,z)W_{mn}(x_1,z_1)}{M_{mn}(\omega_{mn}^2-\omega^2)} \tag{7}$$

From Eq.(6), one can further obtain

$$W_m(x,z,x_1,z_1)=\sum_{m,n=1}^{\infty}\frac{W_{mn}(x,z)\theta_{mn}(x_1,z_1)}{M_{mn}(\omega_{mn}^2-\omega^2)}M,\ \theta_p(x,z,x_1,z_1)=\sum_{m,n=1}^{\infty}\frac{\theta_{mn}(x,z)W_{mn}(x_1,z_1)}{M_{mn}(\omega_{mn}^2-\omega^2)}P,$$

$$\theta_m(x,z,x_1,z_1)=\sum_{m,n=1}^{\infty}\frac{\theta_{mn}(x,z)\theta_{mn}(x_1,z_1)}{M_{mn}(\omega_{mn}^2-\omega^2)}M. \tag{8}$$

where M is a moment at the point (x, z, x_1, z_1), $W_m(x, z)$ is the flexural displacement induced by the moment M, and $\theta_p(x, z)$ is the rotation angle induced by the point force $P\delta(x_1, z_1)$. In Eq.(8), $\theta_{mn}(x, z)$ is computed according to

$$\theta_{mn}(x, z) = \frac{\partial W_{mn}(x, z)}{\partial x}.$$

Similarly, from Eq.(8), one can have the FRFs between the force/moment and the displacement/angle, i.e.

$$H_{wm}(x, z, x_1, z_1) = \sum_{m,n=1}^{\infty} \frac{W_{mn}(x, z)\theta_{mn}(x_1, z_1)}{M_{mn}(\omega_{mn}^2 - \omega^2)}, \quad H_{\theta p}(x, z, x_1, z_1) = \sum_{m,n=1}^{\infty} \frac{\theta_{mn}(x, z)W_{mn}(x_1, z_1)}{M_{mn}(\omega_{mn}^2 - \omega^2)},$$

$$H_{\theta m}(x, z, x_1, z_1) = \sum_{m,n=1}^{\infty} \frac{\theta_{mn}(x, z)\theta_{mn}(x_1, z_1)}{M_{mn}(\omega_{mn}^2 - \omega^2)}. \tag{9}$$

2.2 FRFs associated with the longitudinal vibration of the shaft

Longitudinal vibration equation of the shaft in the free-free boundary condition can be described as [19]

$$\rho A \frac{\partial^2 u(\bar{x}, t)}{\partial t^2} - EA\nabla^2 u(\bar{x}, t) = f(\bar{x}, t) \tag{10}$$

where $\nabla^2 = \frac{\partial^2}{\partial \bar{x}^2}$, E is the modulus of elasticity, ρ the mass density, A the cross section area of the shaft, $u(\bar{x}, t)$ the longitudinal displacement, $f(\bar{x}, t)$ the load acting on the shaft in the longitudinal direction.

Suppose $u(\bar{x}, t) = U(\bar{x})e^{j\omega t}$, $f(\bar{x}, t) = F(\bar{x})e^{j\omega t}$ and substitute them into Eq.(10), one has

$$-\rho A\omega^2 U(\bar{x}) - EA\nabla^2 U(\bar{x}) = F(\bar{x}) \tag{11}$$

Natural frequencies and mode shapes satisfy the characteristic equation, i.e.

$$\rho A\omega_n^2 U_n(\bar{x}) + EA\nabla^2 U_n(\bar{x}) = 0, \quad n \geq 0 \tag{12}$$

where ω_n, $U_n(\bar{x})$ are natural frequencies and mode shapes, respectively. Similarly, the amplitude of longitudinal displacements can be expressed in terms of these natural modes, i.e.

$$U(\bar{x}) = \sum_{n=0}^{\infty} c_n U_n(\bar{x}) \tag{13}$$

In Eqs.(12) and (13), ω_n, $U_n(\bar{x})$ are given by

$$\omega_n = \sqrt{\frac{E}{\rho}}\frac{n\pi}{L}, \quad U_n(\bar{x}) = \sqrt{2}\cos\frac{n\pi\bar{x}}{L} \tag{14}$$

Substituting Eq.(13) into Eq.(11) and taking into account orthogonality of mode shapes, one can arrive at

$$(K_n - M_n\omega^2)U_n = F_n \tag{15}$$

where $M_n = \rho AL(n \geq 1)$, $M_0 = 2\rho AL$, $K_n = M_n\omega_n^2$, $F_n = \int_0^L F(\bar{x})U_n(\bar{x})d\bar{x}$. Combining Eqs.(13) and (15) yields

$$U(\bar{x}) = \sum_{n=0}^{\infty} \frac{U_n(\bar{x})F_n}{M_n(\omega_n^2 - \omega^2)} \tag{16}$$

According to Eq.(16), when $F(\bar{x}) = F\delta(\bar{x})$ is a point force, the FRF between the force and the displacement can be given as

$$H_{uf}(\bar{x}, \bar{x}_1) = \sum_{n=0}^{\infty} \frac{U_n(\bar{x})U_n(\bar{x}_1)}{M_n(\omega_n^2 - \omega^2)} \tag{17}$$

2.3 FRFs associated with the lateral vibration of the shaft

Lateral vibration equation of the shaft in the free-free boundary condition can be described as [19]

$$EJ\nabla^4 w_q(\bar{x},t)+\rho A\frac{\partial^2 w_q(\bar{x},t)}{\partial t^2}=q(\bar{x},t) \tag{18}$$

where $\nabla^4=\frac{\partial^4}{\partial \bar{x}^4}$, E is the modulus of elasticity, J the area moment of inertial, ρ the mass density, A the cross section area of the shaft, $w_q(\bar{x},t)$ the lateral displacement, $q(\bar{x},t)$ the lateral load acting on the shaft.

Suppose $w_q(\bar{x},t)=W(\bar{x})e^{j\omega t}$, $q(\bar{x},t)=Q(\bar{x})e^{j\omega t}$ and substitute them into Eq.(18), one can arrive at

$$EJ\nabla^4 W(\bar{x})-\rho A\omega^2 W(\bar{x})=Q(\bar{x}) \tag{19}$$

Natural Frequencies and mode shapes satisfy the following characteristic equation

$$EJ\nabla^4 W_n(\bar{x})-\rho A\omega_{bn}^2 W_n(\bar{x})=0,\quad n\geq 0 \tag{20}$$

where ω_{bn}, $W_n(\bar{x})$ are natural frequencies and mode shapes, respectively. The amplitude of lateral displacements can be expressed in terms of these natural modes, i.e.

$$W(\bar{x})=\sum_{n=0}^{\infty} b_n W_n(\bar{x}) \tag{21}$$

In Eqs.(20) and (21), ω_{bn} are given by

$$\omega_{b0}=\omega_{b1}=0\,,\omega_{bn}=\beta_n^2\sqrt{\frac{EJ}{\rho A}}\,,n\geq 2$$

where β_n satisfies $1-\cosh\left(\beta_n L\right)\cos\left(\beta_n L\right)=0$, L is the length of the shaft, and $W_n(\bar{x})$ are given by

$$W_0(\bar{x})=1,\ W_1(\bar{x})=2\bar{x}/L-1,\ W_n(\bar{x})=\cosh\left(\beta_n\bar{x}\right)+\cos\left(\beta_n\bar{x}\right)+\gamma_n\left(\sinh\left(\beta_n\bar{x}\right)+\sin\left(\beta_n\bar{x}\right)\right),\ n\geq 2 \tag{22}$$

where γ_n satisfies $\gamma_n=-\frac{\cosh\left(\beta_n L\right)-\cos\left(\beta_n L\right)}{\sinh\left(\beta_n L\right)-\sin\left(\beta_n L\right)}$.

Substituting Eq.(21) into Eq.(19) and taking into account orthogonality of mode shapes, one can have

$$(K_{bn}-\omega^2 M_{bn})W_n(\bar{x})=Q_n \tag{23}$$

where $Q_n=\int_0^L W_n(\bar{x})Q(\bar{x})$, $M_{bn}=\int_0^L \rho A W_n^2(\bar{x})d\bar{x}$, $K_{bn}=\omega_{bn}^2 M_{bn}$. Combining Eqs.(21) and (23), one can have

$$W(\bar{x})=\sum_{n=0}^{\infty}\frac{W_n(\bar{x})Q_n}{M_n(\omega_{bn}^2-\omega^2)} \tag{24}$$

According to Eq.(24), when $Q(\bar{x})=Q\delta(\bar{x})$ is a point force, the FRF between the force and the lateral displacement can be given as

$$H_{wq}(\bar{x},\bar{x}_1)=\sum_{n=0}^{\infty}\frac{W_n(\bar{x})W_n(\bar{x}_1)}{M_n(\omega_{bn}^2-\omega^2)}Q \tag{25}$$

Similarly, if the load is a point moment acting at $\bar{x}_1$ on the shaft, one can further have the following relationship:

$$H_{wt}(\bar{x},\bar{x}_1)=\sum_{n=0}^{\infty}\frac{W_n(\bar{x})\theta_n(\bar{x}_1)}{M_n(\omega_{bn}^2-\omega^2)}T \tag{26}$$

where T is a moment and $\theta_n(\bar{x}_1)$ the rotation angle of the shaft at $\bar{x}_1$.

2.4 FRF synthesis

To obtain the vibration equation of the coupled system, FRF synthesis is carried out on the basis of the derived FRFs given by Eqs.(7), (9), (17), (25) and (26). Fig.2 illustrates displacements and forces existing in the coupled system.

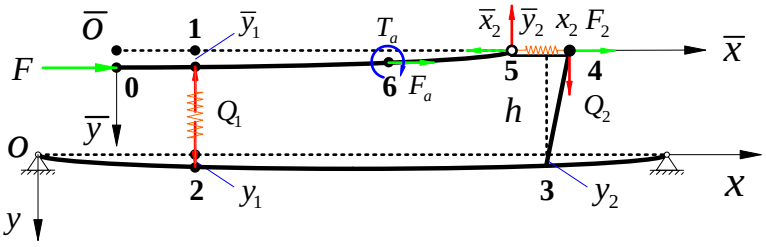

Fig.2 Forces and displacements

In the figure, F is an external disturbance force acting in the longitudinal direction, Q_1 is an internal force generated by the lateral spring and acts on the shaft and the plate, F_2 is an internal force generated by the longitudinal spring and acts on the shaft and the joint, Q_2 is also an internal force caused by the interaction between the shaft and the joint. $\overline{x}_2$ and x_2 are longitudinal displacements of the shaft and the joint, respectively. $\overline{y}_1$ and y_1 are lateral displacements of the shaft and the plate, respectively. y_2 is the flexural displacement of the plate at the rigid joint. F_a is the control force and T_a is a moment relating to actuation.

The displacement at Point 4 is caused by Q_1, Q_2 and F_2, therefore x_2 can be represented in terms of these forces and the corresponding FRFs, i.e.

$$H_{\theta p}(3,2)Q_1h + H_{\theta p}(3,3)Q_2h + H_{\theta m}(3,3)F_2h^2 = x_2 \tag{27}$$

where $H_{\theta p}(3,2)$ is the FRF between the force at Point 2 and the rotation angle at Point 3, $H_{\theta p}(3,3)$ the FRF between the force and the rotation angle at Point 3, and $H_{\theta m}(3,3)$ the FRF between the moment and the rotation angle at Point 3. Similarly, the displacement at Point 3 is also caused by Q_1, Q_2 and F_2, and the following equation holds:

$$H_{wp}(3,2)Q_1 + H_{wp}(3,3)Q_2 + H_{wm}(3,3)F_2h = y_2 \tag{28}$$

where $H_{wp}(3,2)$ is the FRF between the force at Point 2 and the displacement at Point 3, $H_{wp}(3,3)$ the FRF between the force and the displacement at Point 3, and $H_{wm}(3,3)$ the FRF between the moment and the displacement at Point 3. For the displacement at Point 2, there exists a similar relationship, i.e.

$$H_{wp}(2,2)Q_1 + H_{wp}(2,3)Q_2 + H_{wm}(2,3)F_2h = y_1 \tag{29}$$

where $H_{wp}(2,2)$ is the FRF between the force and the displacement at Point 2, $H_{wp}(2,3)$ the FRF between the force at Point 3 and the displacement at Point 2, and $H_{wm}(2,3)$ the FRF between the moment at Point 3 and the displacement at Point 2. For the shaft, the longitudinal displacement at Point 5 can be represented by

$$H_{uf}(5,0)F + H_{uf}(5,6)F_a - H_{uf}(5,5)F_2 = \overline{x}_2 \tag{30}$$

where $H_{uf}(5,0)$ is the FRF between the disturbance force and the displacement at Point 5, $H_{uf}(5,5)$ the FRF between the internal force and the displacement at Point 5, $H_{uf}(5,6)$ the FRF between the control force and the displacement at Point 5. The lateral displacements at Points 1and 5 can be represented by

$$H_{wt}(1,6)T_a - H_{wq}(1,1)Q_1 - H_{wq}(1,5)Q_2 = \overline{y}_1 \tag{31}$$

$$H_{wt}(5,6)T_a - H_{wq}(5,1)Q_1 - H_{wq}(5,5)Q_2 = \overline{y}_2 \tag{32}$$

where $H_{wq}(1,1)$ is the FRF between the force and the displacement at Point 1, $H_{wq}(1,5)$ the FRF between the force at Point 5 and the displacement at Point 1, $H_{wq}(5,1)$ the FRF between the force at Point 1 and the displacement at Point 5, $H_{wq}(5,5)$ the FRF between the force and the displacement at Point 5, $H_{wt}(1,6)$ the FRF between the moment at Point 6 and the displacement at Point 1, $H_{wt}(5,6)$ the FRF between the moment at Point 6 and the displacement at Point 5.

Apart from Eqs.(26)-(31), there exist equilibrium and continuity conditions for the forces and displacements, i.e.

$$k_t(\bar{x}_2 - x_2) = F_2 \tag{33}$$

$$k_s(\bar{y}_1 - y_1) = Q_1 \tag{34}$$

$$\bar{y}_2 - y_2 = 0 \tag{35}$$

Eq.(30) and Eq.(33) implies

$$H_{uf}(5,0)F + H_{uf}(5,6)F_a - H_{uf}(5,5)F_2 - F_2 / k_t = x_2 \tag{36}$$

Eq.(31) and Eq.(34) implies

$$H_{wt}(1,6)T_a - H_{wq}(1,1)Q_1 - H_{wq}(1,5)Q_2 - Q_1 / k_s = y_1 \tag{37}$$

Eq.(32) and Eq.(35) implies

$$H_{wt}(5,6)T_a - H_{wq}(5,1)Q_1 - H_{wq}(5,5)Q_2 = y_2 \tag{38}$$

From Eqs.(27)-(32) and (36)-(38), one can have

$$\begin{bmatrix} H_{\theta p}(3,2)h & H_{\theta p}(3,3)h & H_{\theta m}(3,3)h^2 + H_{uf}(5,5) + 1/k_t \\ H_{wp}(3,2) + H_{wq}(5,1) & H_{wp}(3,3) + H_{wq}(5,5) & H_{wm}(3,3)h \\ H_{wp}(2,2) + H_{wq}(1,1) + 1/k_s & H_{wp}(2,3) + H_{wq}(1,5) & H_{wm}(2,3)h \end{bmatrix} \begin{Bmatrix} Q_1 \\ Q_2 \\ F_2 \end{Bmatrix} = \begin{Bmatrix} H_{uf}(5,0)F \\ 0 \\ 0 \end{Bmatrix} + \begin{Bmatrix} H_{uf}(5,6)F_a \\ H_{wt}(5,6)T_a \\ H_{wt}(1,6)T_a \end{Bmatrix} \tag{39}$$

According to Eq.(39), the internal forces can be determined provided F, F_a, T_a are known, and FRFs of the coupled system are computed on the basis of these internal forces. One can compute FRFs of the coupled system corresponding to the disturbance force by setting $F_a = 0$ and $T_a = 0$, and FRFs corresponding to the control force by setting $F = 0$ and $T_a = 0$.

3 A numerical example

Consider the shaft-plate coupled system, which is shown in Fig.1. Parameters of the system are listed in Table 1. Eq.(39) is used to derive natural frequencies of the coupled system, which are listed in Table 2. For the purpose of comparison, frequencies are also computed by the finite element method (FEM) and listed in Table 3. The discrepancy is within 5%. It is worthy of mentioning that the fist natural frequency can also be estimated from a single-degree-of-freedom system that is composed of the shaft and the longitudinal spring and the estimate is 10.2Hz.

Table 1 Parameters used in computation

Notation	-	Notation	-	Notation	-	Notation	-	Notation	-
ρ (kg/m^3)	7850	L (m)	1.0	k_s (N/m)	4×10^5	l_x (m)	1.2	l_s (m)	0.2
E (N/m^2)	2.1×10^{11}	h (m)	0.1	k_t (N/m)	1×10^4	l_z (m)	1.0	l_a (m)	0.6
ν	0.3	$*d$ (m)	0.02	δ (m)	0.006	-	-	l_b (m)	0.2

$*d$ -Diameter of the shaft

Table 2 Natural frequencies (Hz)

Order	1	2	3	4	5	6	7	8	9	10	11	12
Frequency	10.1	24.4	58.1	79.7	116.5	143.9	164.9	176.5	203.2	227.1	270.9	297.3

Table 3 Natural frequencies (Hz) computed by FEM

Order	1	2	3	4	5	6	7	8	9	10	11	12
Frequency	10.1	24.4	58.7	82.7	113.9	143.5	171.6	177.3	214.5	226.7	270.9	296.9

FRFs between the disturbance force and the displacements at Points 4, 2 and 3 are illustrated respectively in Figs.3 and 4 (In the computation of FRFs, a small damping ratio 0.001 is introduced to the system). As can be seen from these figures, at some natural frequencies, the longitudinal response is not noticeable, which implies that the impedance associated with rotation at the joint is relatively larger and vibration of the shaft is mainly composed of lateral vibration. Moreover, if the internal forces are examined, it can be found that amplitude of the longitudinal reaction force at these natural frequencies is less discernible than the lateral reaction forces, as shown in Figs.5 and 6. When the lateral spring stiffness varies, the longitudinal response and reaction force at Point 4 will vary accordingly, as shown in Figs.7 and 8. In Fig.7, the dominant peak of an FRF at a fixed k_t occurs at the frequency that corresponds to a longitudinal vibration mode of the shaft and this frequency is determined by the combination of k_t and the equivalent stiffness associated with the longitudinal deflection at Point 4, which is approximately 3×10^6 N/m. These frequencies can be roughly estimated and the estimates are 10.2Hz, 31.6Hz and 88.1Hz, which are very close to the exact ones, i.e. 10.1Hz, 31.8Hz

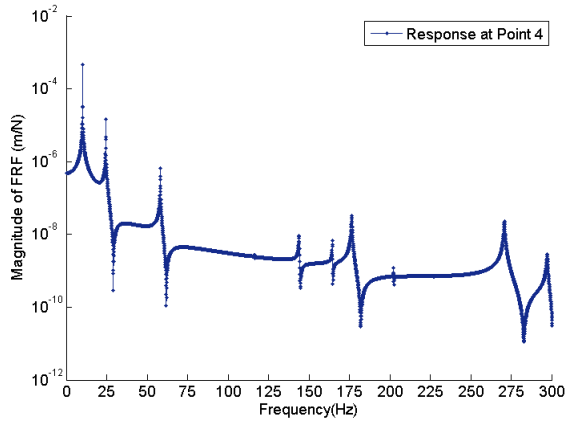

Fig.3 Longitudinal displacement to the unit force F

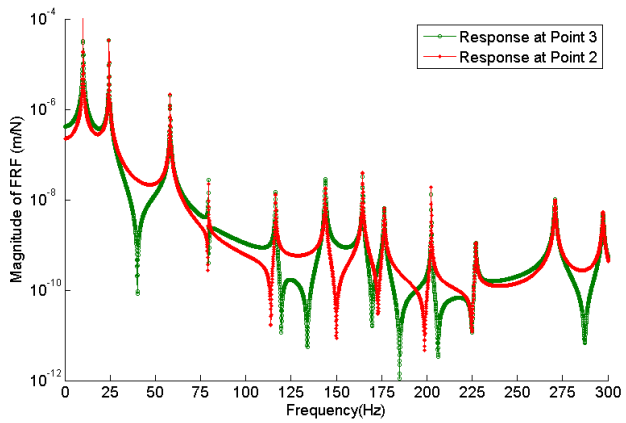

Fig.4 Lateral displacements to the unit force F

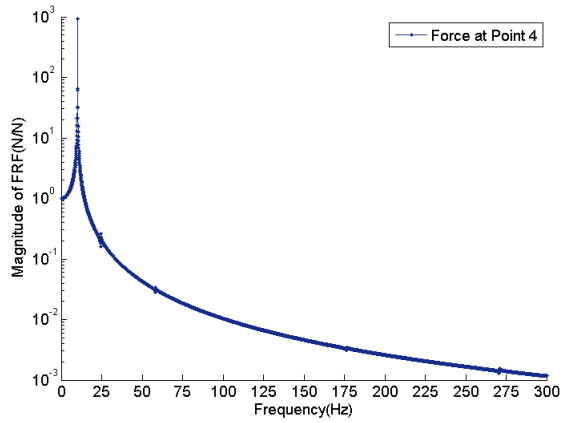

Fig.5 Longitudinal force induced by the unit force F

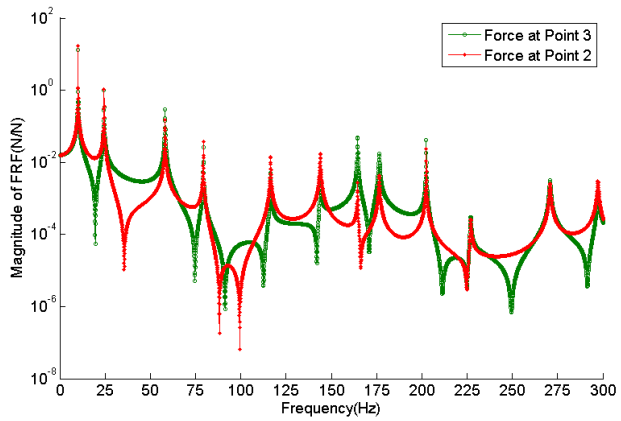

Fig.6 Lateral forces induced by the unit force F

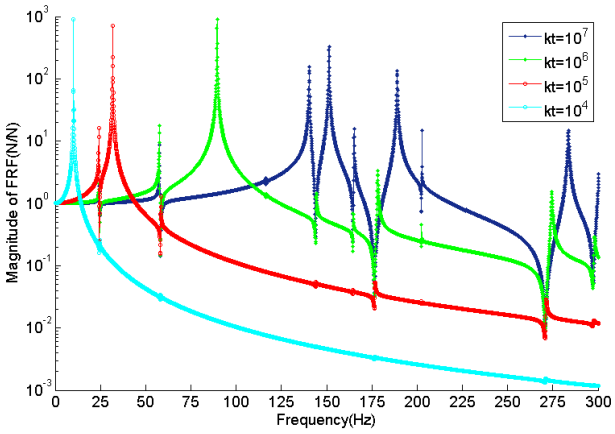

Fig.7 Longitudinal force at Point 4

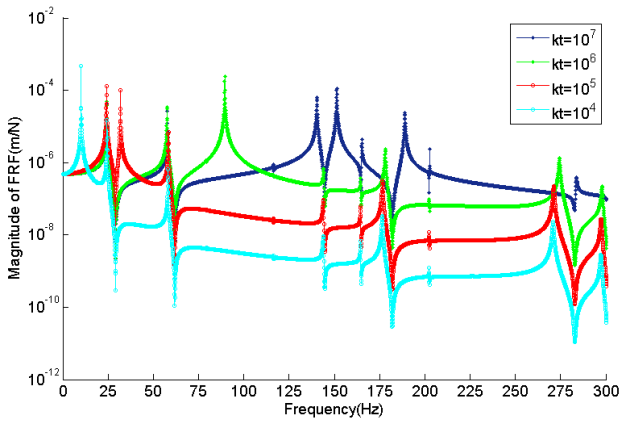

Fig.8 Longitudinal displacement at Point 4

and 89.5Hz. From Fig.8 one can also see an interesting phenomenon that some natural frequencies are insensitive to the variation of k_t. One reason for this phenomenon is that vibrations at these frequencies are dominated by the flexural modes of the plate, whose modal mass is approximately 56kg and much larger than that of the shaft (2.5kg), and for some insensitive modes the relative longitudinal displacement between the shaft and the joint is very small.

Illustrated in Fig.9 are the first three mode shapes, from which one can see that the longitudinal displacement is related to the rotation angle of the joint except for the first mode. Therefore, the bigger the rotation angle, the stronger the influence of the longitudinal spring on the coupled modes.

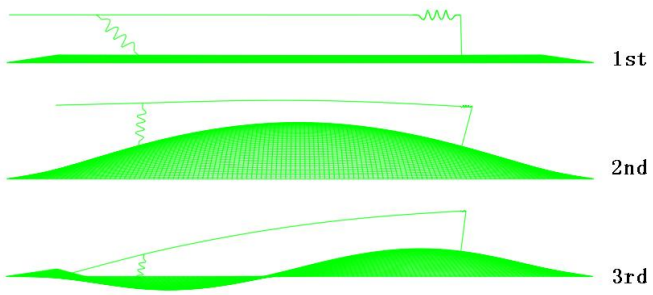

Fig.9 Mode shapes

Now consider FRFs associated with the longitudinal control force F_a, which acts at Point 6 as shown in Figs.1 and 2. Suppose $k_t = 10^7$ N/m and compute FRFs according to Eq.(39). The results are shown in Figs.10 and 11. Apparently, F_a and F produce nearly the same responses, which implies that F_a can completely cancel the effect of F. This property is guaranteed by the longitudinal rigidity of the shaft. Hence, if the longitudinal displacement x_2 at Point 4 is suppressed, it can be expected that vibration at the plate will be suppressed as well. However, if the control force deviates a little from the center of the shaft, there will be a moment acting on the shaft, which can induce lateral vibration in the shaft.

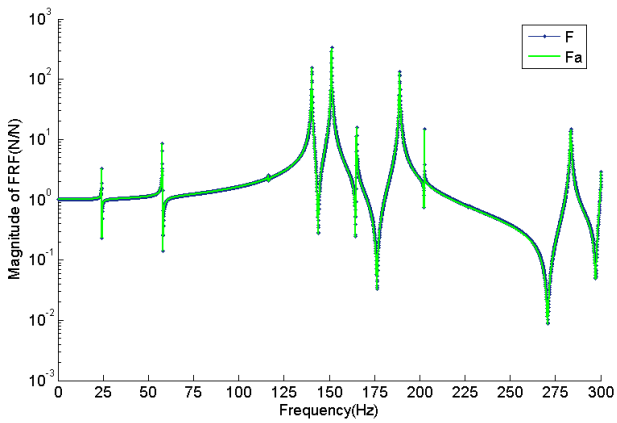

Fig.10 Longitudinal force at Point 4

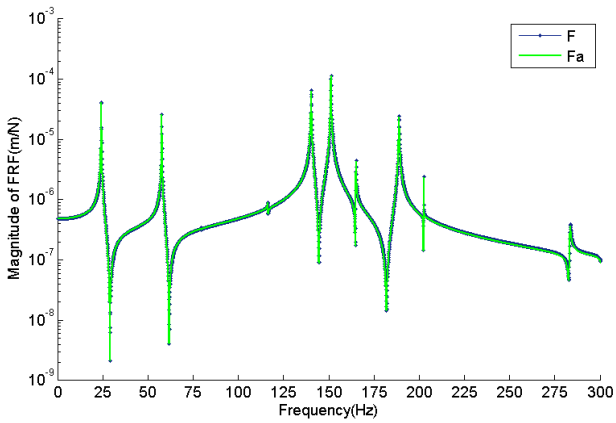

Fig.11 Longitudinal displacement at Point 4

4 Active control of the longitudinal vibration

It is straightforward to carry out active control for such a coupled system under periodic excitation if it is time-invariant. However, active control will become difficult when the longitudinal spring is not a constant but varies piecewisely in a large range, say, 10^4-10^7 N/m. In this circumstance, FRFs associated with the control force will vary with the stiffness, which makes it necessary to use time-varying strategies if time-varying dynamic models are needed in the construction of controllers. However, new problems will arise in the identification of models for such a piecewisely time-varying system because identification should be conducted online in parallel with the control action. To overcome this problem, a new control method is proposed to cancel periodic disturbances without any dynamic model of the coupled system. This controller is constructed on the adaptive feedback control scheme, which in fact combines the LMS algorithm and the tracking filtering technique. The structure of the controller is shown in Fig.12, where the saturation unit is utilized to restrict the controller's output, d(k) represents the disturbance, z(k) is the response induced by the actuator and e(k) the resultant longitudinal response at the reference point, for instance, Point 4.

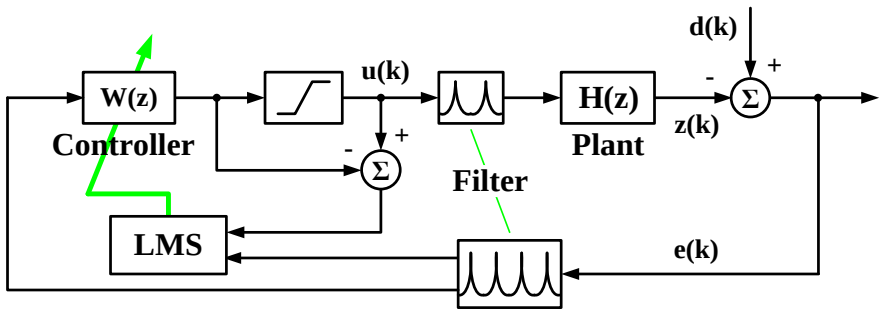

Fig.12 The proposed adaptive feedback control scheme

In this study, the fundamental frequency of the disturbance d(k) is assumed to be known or can be measured accurately. In this circumstance, the center frequencies of tracking filters can be set exactly to this frequency and its multiples, but for simplicity of discussion, suppose there is only one harmonic disturbance and accordingly only one tracking filter is needed. The tracking filter is a second order band-pass filter, and its transfer function in the z-domain can be described as [20]

$$\Phi(z) = \left(b_0 + b_2 z^{-2}\right)\left(1 + a_1 z^{-1} + a_2 z^{-2}\right)^{-1} \tag{40}$$

where $a_1 = -2\exp(-\zeta\omega / f_s)\cos(\sqrt{1-\zeta^2}\,\omega / f_s)$, $a_2 = \exp(-2\zeta\omega / f_s)$, $b_0 = (1-\exp(-2\zeta\omega / f_s))/2$, $b_2 = -b_0$, f_s is the sampling frequency, ω the center frequency of the tracking filter and ζ the damping ratio.

The controller shown in Fig.12 is a finite impulse response (FIR) filter, coefficients of which are adjusted according to the least mean square (LMS) algorithm. Since there is a saturation unit following the FIR controller, it is necessary to modify the LMS algorithm to accommodate this change. The modified algorithm is presented as follows [21].

The coefficients of the FIR controller $W(z)$ are updated according to

$$\boldsymbol{w}_{k+1} = f_u \boldsymbol{w}_k + \mu \frac{f_u \varepsilon_k + (1-f_u)\boldsymbol{w}_k^T \boldsymbol{\rho}_k}{\gamma + \|\boldsymbol{\rho}_k\|^2} \boldsymbol{\rho}_k \tag{41}$$

where $\boldsymbol{w}_k$ is a vector of N+1 elements, $\boldsymbol{\rho}(k) = [\varepsilon_k, \varepsilon_{k-1}, \cdots, \varepsilon_{k-N}]^T$ and ε_k is the response of the tracking filter $\Phi(z)$ to the input e_k, μ is a constant, $\gamma > 0$, $f(u)$ is a sigmoid function and $f_u = f_u(\boldsymbol{w}_k^T \boldsymbol{\rho}_k)$ is the derivative of $f(u)$ at $u = \boldsymbol{w}_k^T \boldsymbol{\rho}_k$. It should be mentioned that stability of the adaptive feedback cancellation without applying a sigmoid function is not guaranteed because the feedback gain would otherwise tend to approach infinity and render the closed loop sensitive to variation. Although the controller adjusted according to Eq.(41) minimizes the instantaneous error e_k, the saturation unit will create distortion in the output signal u(k). Hence, a tracking filter just following the saturation unit is necessary to get rid of any nonlinear response caused by the distortion. The advantage of using feedback instead of feedforward control is that no reference signal/transducer is necessary.

When using Eq.(41) to carry out feedback control, a new problem arises that dynamics of the control channel (plant) will change the adaptation stability of Eq.(41) because Eq.(41) does not compensate the plant dynamics in the feedback loop. As shown in Fig.13, the phase-frequency characteristics of $\bar{x}_2 / F_a$ vary with the stiffness k_t and the phase jump is nearly $180°$ over certain frequency band. Therefore, μ must change its sign to ensure a correct adaptation direction for $\boldsymbol{w}_k$ when a phase jump occurs due to the variation of k_t. Here, we propose a mechanism that works in parallel with Eq.(41) to guarantee the stability of adaptation of $\boldsymbol{w}_k$.

Consider an energy function that is defined as follows:

$$\bar{E}(t) = \frac{1}{\Delta}\int_{t-\Delta}^{t} \varepsilon^2(\tau)\,d\tau \tag{42}$$

where $\Delta = 2\pi / \omega$. Suppose $\varepsilon(t) = r(t)\sin\omega t$ and varies much slower than $\sin\omega t$, where $r(t)$ is the amplitude of $\varepsilon(t)$, then $\bar{E}(t) \approx r^2(t)/2$. The derivative of $\bar{E}(t)$ with respect to t is approximately $r(t)\frac{dr(t)}{dt}$. Therefore, when $\varepsilon(t) = r(t)\sin\omega t$ increases, the derivative will be positive. This simple property can be used to adjust the sign of the

step size parameter μ. However, $r(t)\frac{dr(t)}{dt}$ implies that the derivative is dependent on the amplitude of a specific signal. To remove this dependency, one can use $\frac{1}{r(t)}\frac{dr(t)}{dt}$ to replace $r(t)\frac{dr(t)}{dt}$. Therefore, for an exponentially varying signal, $\frac{1}{r(t)}\frac{dr(t)}{dt}$ is a time-independent value. On the basis of $\frac{1}{r(t)}\frac{dr(t)}{dt}$, μ is imposed to change its sign and magnitude according to the following mechanism:

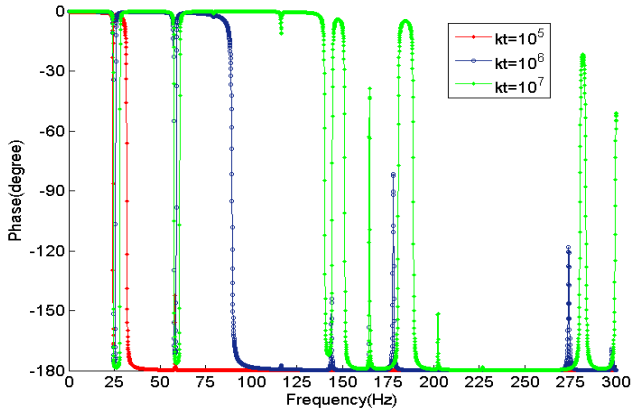

Fig.13 Phase-frequency diagram of $\bar{x}_2 / F_a$

$$\mu = \begin{cases} \mu, \ when \ \ r(t) \le r_0 \\ \mu\kappa(t), \ when \ \ \frac{1}{r(t)}\frac{dr(t)}{dt} \ge 0 \ and \ r(t) > r_0 \\ \mu\left(1 + c_a r(t) / \left(\left|\frac{dr(t)}{dt}\right| + c_b\right)\right), \ when \ \ \frac{1}{r(t)}\frac{dr(t)}{dt} < 0 \ and \ r(t) > r_0 \end{cases} \tag{43}$$

where r_0 is a positive threshold value for $r(t)$, $\kappa(t)$ is a square wave and $-1 \le \kappa(t) \le 1$, $c_a, c_b > 0$. In Eq.(43), $\kappa(t)$ is used to prevent excessive alternation of the sign of μ, $c_a r(t) / \left(\left|\frac{dr(t)}{dt}\right| + c_b\right)$ is used to accelerate the convergence of $\varepsilon(t)$. Eq.(43) implies that μ will continue changing its sign and magnitude until a negative derivative or a sufficient small error is achieved.

5 The longitudinal-lateral vibration control

In this section, vibration control for the shaft-plate system given in Section 2 is discussed on the basis of the structure shown in Fig.12 and Eqs.(40-41) and (43). When conducting active suppression of longitudinal vibration, acceleration at Point 5 is preferably used as the error signal since the associated FRF is nearly a driving point FRF and acceleration response at Point 5 is not attenuated by the longitudinal spring (On the contrary, response at Point 4 is greatly affected by the spring stiffness). Fig.14 shows the variation of $-\omega^2 \bar{x}_2 F_a^{-1}$ (FRF of the control channel) with the spring stiffness.

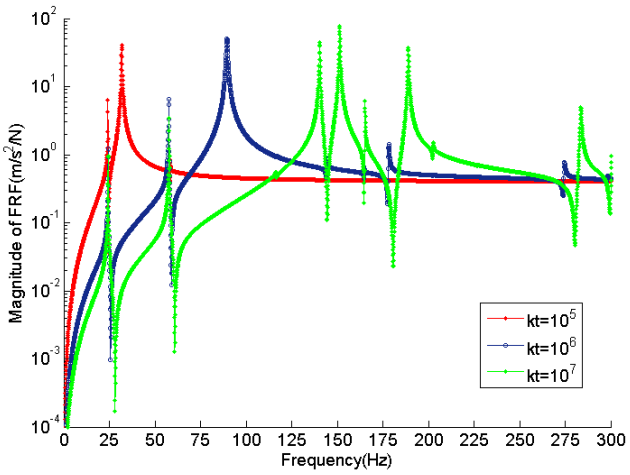

Fig.14 Acceleration responses at Point 5 to the control force F_a

The analytical form of $(j\omega)^2 \bar{x}_2 F_a^{-1}$ needs to be established at first because simulation needs a recursive numerical model of the control channel, i.e. H(z) in Fig.12, which can be obtained by the z-conversion of its counterpart.

5.1 Identification of $\omega^2 \bar{x}_2 F_a^{-1}$

According to the theory of modal analysis, $\bar{x}_2 F_a^{-1}$ can be given in the following form:

$$\bar{x}_2 F_a^{-1} = \sum_k \frac{\omega_k^2 \chi_k}{-\omega^2 + j2\zeta_k \omega\omega_k + \omega_k^2} \tag{44}$$

where $\chi_k > 0$, ζ_k is the damping ratio of the kth mode, ω_k the frequency of the kth mode. Since $\zeta_k \approx 0.001$ and the unknown parameter is χ_k only, one can use the least squares method to find χ_k. Therefore, let $\zeta_k = 0.001$ and write equations at the discrete frequencies according to Eq.(44) and the known natural frequencies, one has

$$\begin{bmatrix} |h_1(\omega_1)| & |h_2(\omega_1)| & \cdots & |h_\alpha(\omega_1)| \\ |h_1(\omega_2)| & |h_2(\omega_2)| & \cdots & |h_\alpha(\omega_2)| \\ \vdots & \vdots & \ddots & \vdots \\ |h_1(\omega_\beta)| & |h_2(\omega_\beta)| & \cdots & |h_\alpha(\omega_\beta)| \end{bmatrix} \begin{Bmatrix} \chi_1 \\ \chi_2 \\ \vdots \\ \chi_\alpha \end{Bmatrix} = \begin{Bmatrix} |\bar{x}_2 F_a^{-1}(\omega_1)| \\ |\bar{x}_2 F_a^{-1}(\omega_2)| \\ \vdots \\ |\bar{x}_2 F_a^{-1}(\omega_\beta)| \end{Bmatrix} \tag{45}$$

where $h_k(\omega) = \omega_k^2 \left(-\omega^2 + j2\zeta_k \omega\omega_k + \omega_k^2\right)^{-1}$, $k = 1 \sim \alpha$, $\beta \sim \alpha$. From Eq.(45), an approximation of $(j\omega)^2 \bar{x}_2 F_a^{-1}$ can be obtained. Fig.15 is the result of approximation ($k_t = 10^7$ N/m) and the comparison indicates a good agreement.

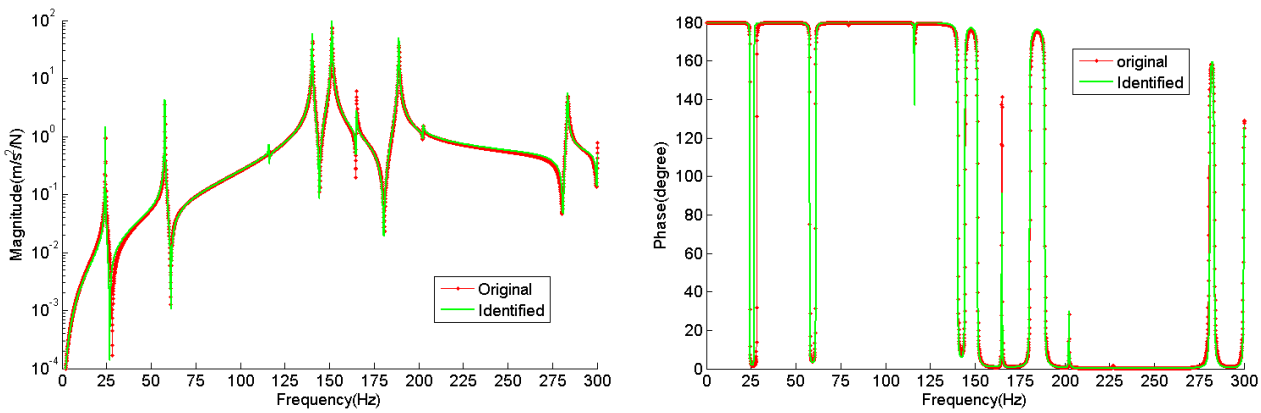

Fig.15 Identified FRF -$(j\omega)^2 \bar{x}_2 F_a^{-1}$

With the decomposition of $(j\omega)^2 \bar{x}_2 F_a^{-1}$, the response of $(j\omega)^2 \bar{x}_2 F_a^{-1}$ can be calculated as the summation of the responses of a series of single-degree-of-freedom systems.

5.2 Performance of the control method

The effectiveness of Eqs.(40), (41) and (43) is examined in this section with the identified plant models described by Eq.(44). In the first simulation, stiffness of the longitudinal spring is assumed to jump between $k_t = 10^5$ N/m and $k_t = 10^7$ N/m. As a result, the change of magnitude of $\omega^2 \bar{x}_2 F_a^{-1}$ is like that in Fig.14 and the phase change is similar to that in Fig.13. Parameters in Eq.(43) are $\mu = 10$, $r_0 = 10^{-5}$, $c_a = 1000$, $c_b = 1$. The excitation frequency is 100Hz and the sampling frequency is 1000Hz. The phase change at 100Hz is about $180°$, which implies possible instability in the closed system if the feedback gain does not change. Fig.16 shows the signals in the controlled system. According to Fig.16(f), one can see that the error signal after control is greatly attenuated, but at the same time, there are also jumps in the controlled signal. In fact, these sharp jumps are caused by the switch of the plant models, which further triggers the prompt changes in the sign of μ, as is shown in Fig.16(c). The alteration of the sign is dependent on the signals in

Figs.16(d) and (e), which are computed according to Eq.(43). When the variation rate of $r(t)$ is negative, a large gain is allowed to accelerate the convergence of the controlled error $\varepsilon(t)$, otherwise the gain remains at a small level so as to reduce the closed loop sensitivity. As can be seen in Fig.16(a), the control signal also changes when the plant model is different, the signal $u(t)$ is smaller for the model with $k_t = 10^5$ N/m than that for the model with $k_t = 10^7$ N/m.

Consider another case where the model is assumed to keep unchanged but the excitation frequency varies piecewisely from 50Hz to 200Hz. The plant model adopted in simulation corresponds to $k_t = 10^7$ N/m and there are obviously many jumps in its phase-frequency diagram (Fig.13). Parameters in Eq.(43) are changed to $\mu = 30, r_0 = 10^{-5}, c_a = 10000, c_b = 1$. The results are shown in Fig.17, which demonstrates a similar performance of attenuation in the controlled responses at the seven discrete frequencies although phase changes are almost $180°$. However, alteration of the sign of μ is more complicated than the case in Fig.16. μ changes its sign frequently due to the oscillation of $\frac{1}{r(t)}\frac{dr(t)}{dt}$ around zero and this uncertainty in sign is related to the space a specific excitation frequency stands away from lightly vibration modes, which in fact determines the degree of influence of lightly damped modes on the filtered error signal. This difficulty is caused by the uncompensated dynamics of the plant model. Therefore, large damping ratios will be favorable to the implementation of control.

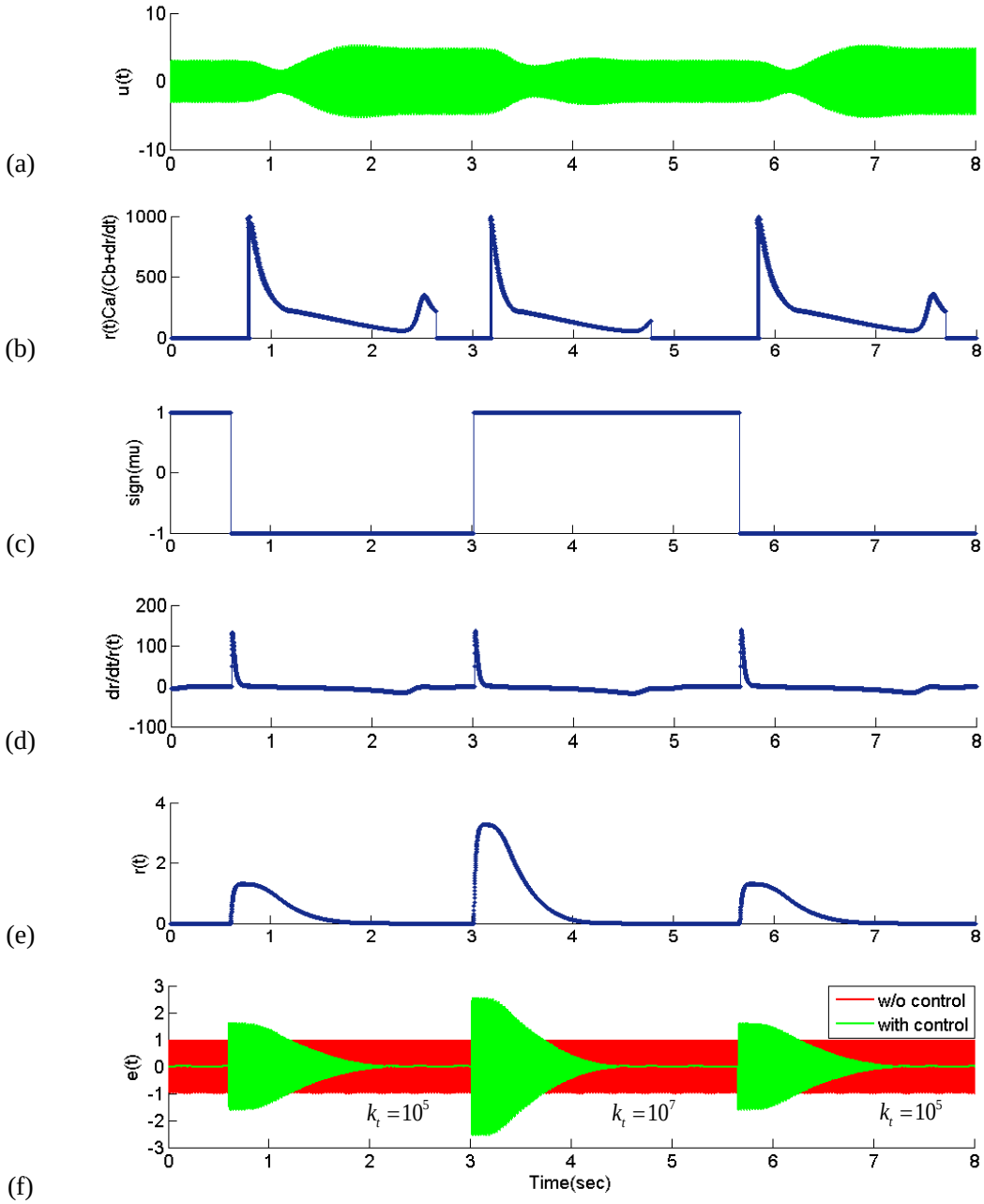

Fig.16 Signals in the controlled system (switch of plant models)

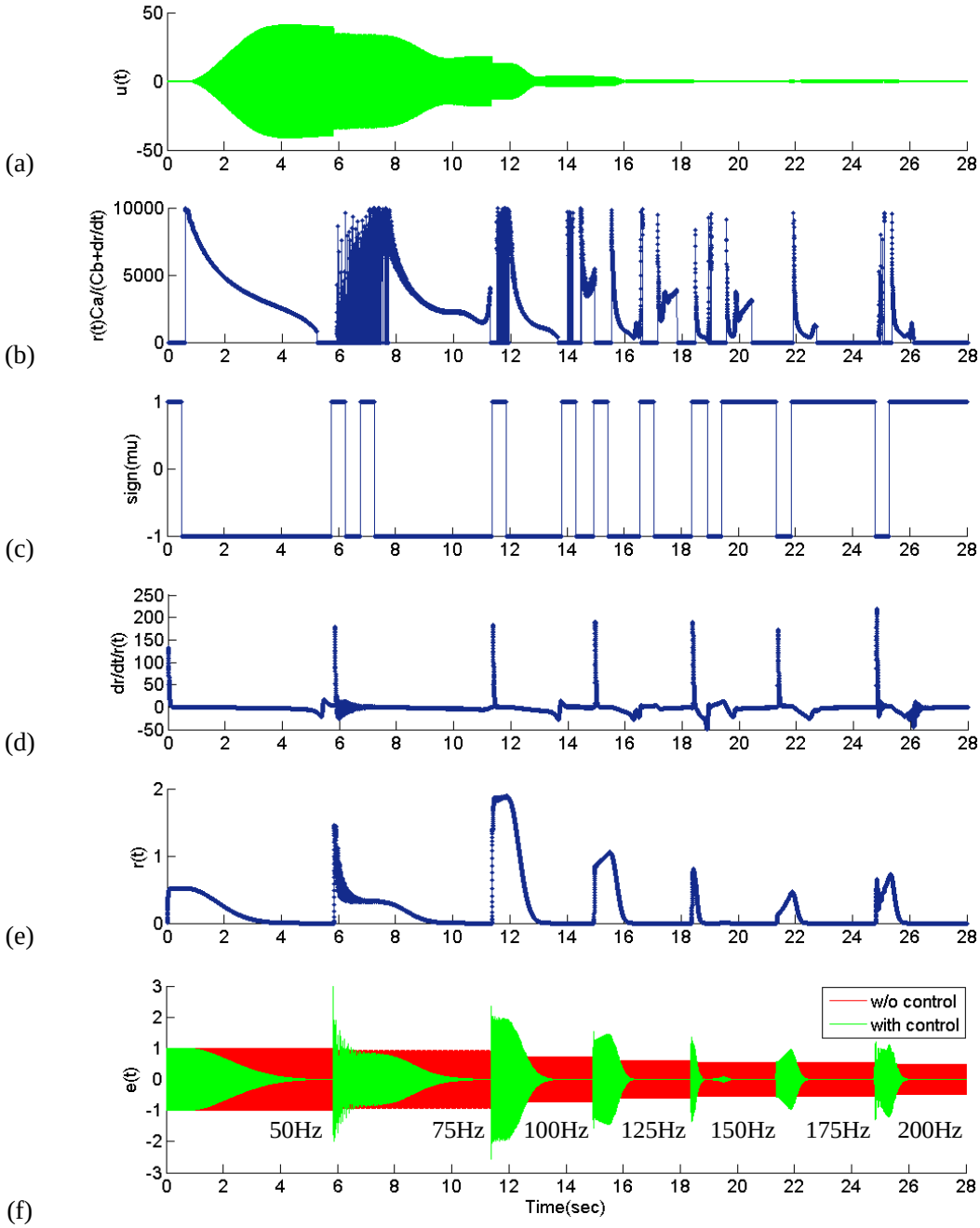

Fig.17 Signals in the controlled system (no switch of plant models but excitation frequencies)

5.3 Reduction of vibration in the coupled system

In this section, vibration of the coupled system after active longitudinal vibration control is further discussed on the basis of the validated model and the control method. Figures 16 and 17 have demonstrated that vibration at Point 5 can be reduced by exerting an active force along the shaft axis. In fact, notice that $H_{uf}(5,0) = H_{uf}(5,6)$ within certain range of frequency and Eq.(39) holds, it can be deduced that $F_2 = Q_1 = Q_2 = 0$ provided $F + F_a = 0$, which further implies the longitudinal displacement of the shaft $\overline{x}_2 = 0$ and the plate's vibration induced by F_2, Q_1, Q_2 will be suppressed as well. To demonstrate it, consider another simulation for the system under excitation of three harmonic disturbances. Suppose the disturbance force F comprises three harmonics, which are at 50Hz, 75Hz and 100Hz, and the error signal is contaminated by zero mean white noise with variance 10^{-5}. The plant model corresponds to $k_t = 10^7$ N/m and $\mu = 30, r_0 = 10^{-5}, c_a = 10^4, c_b = 1$. Three tracking filters with $\zeta = 10^{-4}$ are used to decompose the error signal and three independent control units are also used to deal with each harmonic. The number of weights for each control unit is 8. Fig.18 illustrates the responses of Point 5 before and after control. As can be seen in this figure, the three components

are noticeably suppressed. The three components are induced respectively by the corresponding forces 1.80N, 1.09N and 0.39N. For comparison, F , F_a and F_2 are given in Fig.19, from which one can see that F_a attempts to approach F and cancel its effect and F_2 is reduced as implied by Eq.(39). The same results apply to the forces Q_1 , Q_2 .

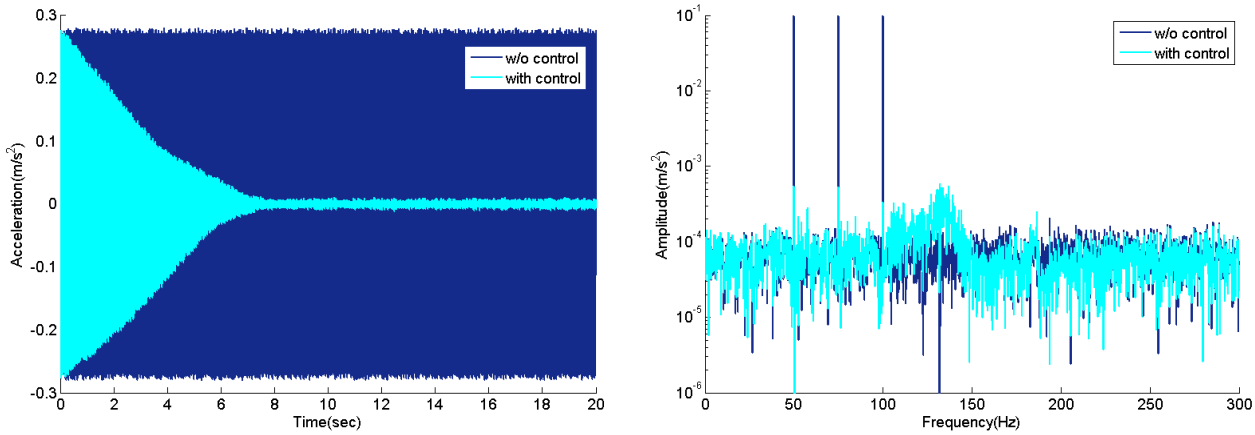

Fig.18 Comparison of acceleration responses at Point 5 with/without control

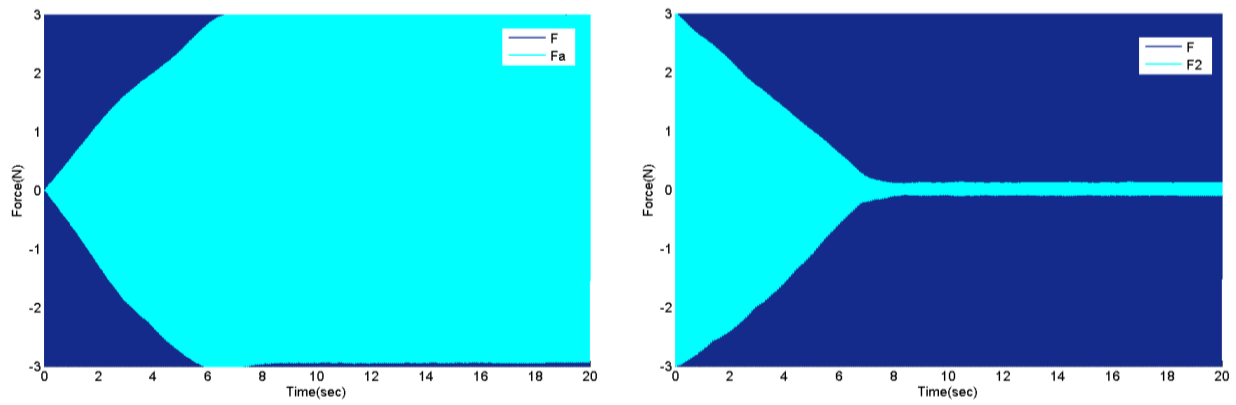

Fig.19 Forces in the controlled system

However, if the active force F_a deviates from the shaft axis, the moment T_a caused by F_a will result in lateral vibration in the plate. To illustrate how the moment affects the plate's vibration, FRFs associated with T_a are computed and shown in Fig.20, where $k_t = 10^7$ N/m. Notice that there exists a relationship between T_a and F_a , that is $T_a = e_a F_a$, where e_a is the distance of deviation of F_a from the shaft axis, the influence of T_a is actually weaker when $e_a \le 0.01\text{m}$. It can be seen from the figure that F_a has a stronger influence on F_2 than T_a and the influence of T_a on Q_1 and Q_2 is also weaker than F_a except at some frequencies, such as around 80Hz, comparable to that of F_a and accordingly cannot be neglected. Therefore, it is necessary to keep T_a as small as possible, otherwise lateral vibration will be induced in the plate even though F_a cancels completely the effect of F .

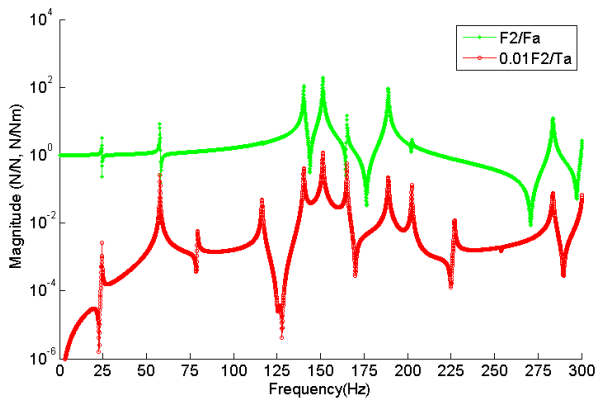

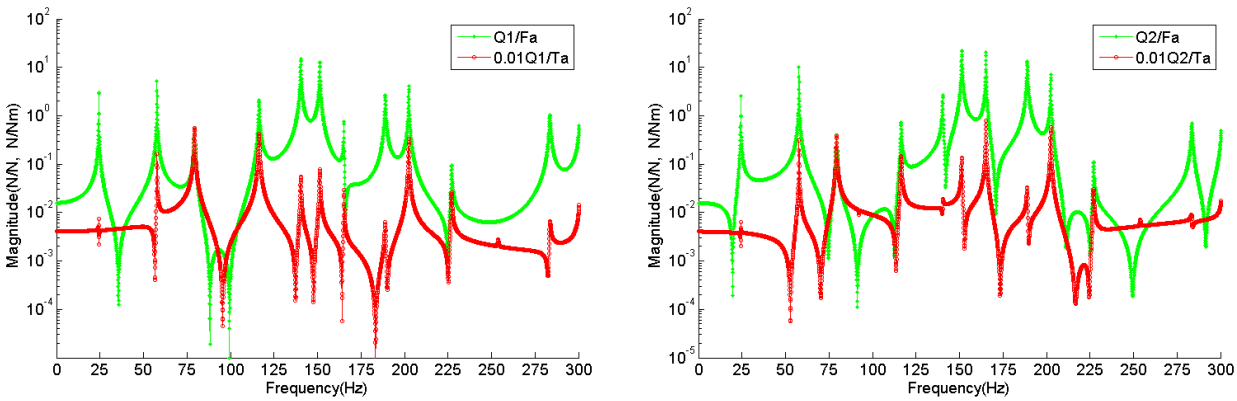

Fig.20 Comparison of the influence of F_a and T_a when $e_a \leq 0.01\text{m}$

Therefore, vibration of the coupled system can be reduced theoretically through adaptive longitudinal actuation on the shaft and the deviation of the actuation force from the shaft axis should be restricted to a sufficiently small range.

6 Conclusions

Vibration of the shaft-plate coupled system is composed of longitudinal and lateral vibration. To describe the involved dynamics, a simplified model is established for this system by FRF synthesis. The modeling approach is verified with FEM but preferable to FEM in dynamics analysis. According to the model, the longitudinal force can generate not only axial vibration in the shaft but lateral/flexural vibration in the system through flexible supports. Based on the analysis of dynamics, vibration control via longitudinal actuation on the shaft and the pertinent active control scheme are further studied. The active control scheme is constructed on an adaptive feedback scenario and enhanced with a mechanism for adaptation of the controller's gain in the case of time-varying dynamics induced by changes in the flexible supports. Simulation results have demonstrated that the control scheme with the proposed mechanism is effective in attenuating vibration of the system and sufficient modal damping is favorable to the convergence of control. Axial actuation on the shaft is able to cancel the effect of the longitudinal disturbance acting at the free end of the shaft and consequently reduces the internal forces as well as vibration in the plate. However, deviation of the actuation force from the shaft axis will deteriorate control of lateral vibration and sufficiently small deviation needs to be guaranteed.

Acknowledgements: This work was supported in part by State Key Laboratory of Mechanical system and Vibration (Grant No. MSV-MS-2010-10) and China Scholarship Council (2010-2011).

References

1. A.J.H. Goodwin, The design of a resonance changer to overcome excessive axial vibration of propeller shafting, Transactions of the Institute of Marine Engineers, 1960, 72: 37-63
2. P.G. Dylejko, N.J. Kessissoglou, Y. K. Tso, C.J. Norwood, Optimization of a resonance changer to minimize the vibration transmission in marine vessels, Journal of Sound and Vibration, 2007, 300: 101-116
3. Y. Cao, W. Zhang, Using dynamic absorbers to reduce underwater structural noise due to longitudinal vibration of shafting, Journal of Harbin Engineering University (In Chinese), 2007, 28(7): 747-751
4. S. Merz, Passive and active control of the sound radiated by a submerged vessel due to propeller forces, Ph.D. Thesis of University of New South Wales, Sydney, Australia, 2010
5. D.W. Lewis, P.E. Allaire, P. W. Thomas, Active magnetic control of oscillatory axial shaft vibrations in ship shaft transmission systems, Part 1: System natural frequencies and laboratory scale model, Journal of Tribology ransactions, 1989, 32(2): 170-178
6. S. Merz, R. Kinns, N. Kessissoglou, Structural and acoustic responses of a submarine hull due to propeller forces, Journal of Sound and Vibration, 2009, 325:266-286
7. G. Feng, Study on the stern vibration transmission based on power flow analysis, Ph.D. Thesis (In Chinese) of

Shanghai Jiao Tong University, Shanghai, China, 2010
8. M. Caresta and N. Kessissoglou, Acoustic signature of a submarine hull under harmonic excitation, Applied Acoustics, 2010, 71: 17-31
9. D.W. Lewis, R.R. Humphris, P.W. Thomas, Active magnetic control of oscillatory axial shaft vibrations in ship shaft transmission systems, Part 2: Control analysis and response of experimental system, Journal of Tribology Transactions, 1989, 32(2): 179-188
10. J. Pan, N. Farag, T. Lin and R. Juniper, Propeller induced structural vibration through the thrust bearing. Proceedings of the Annual Conference of the Australian Acoustical Society, 13-15 November, 2002, Adelaide, Australia, 390-399
11. C. Bohn, A. Cortabarria, V. Hartel and K. Kowalczyk, Active control of engine-induced vibrations in automotive vehicles using disturbance observer gain scheduling, Control Engineering Practice, 2004, 12: 1029-1039
12. L. Håkansson, I. Claesson, P.O. Sturesson, Adaptive feedback control of machine-tool vibration based on the filtered-x LMS algorithm, International Journal of Low Frequency Noise, Vibration and Active Control, 1998, 17(4): 199-213
13. I.D. Landau, A. Constantinescu and D. Rey, Adaptive narrow band disturbance rejection applied to an active suspension—an internal model principle approach, Automatica, 2005, 41: 563–574
14. P.R. Pagill, B.Yu, K. Pau, Adaptive control of time-varying mechanical systems: analysis and experiments, IEEE/ASME Transactions on Mechatronics, 2000, 5(4): 410-418
15. E. Duviella, V. Puig, P. Charbonnaud et al., Supervised gain-scheduling multi-model versus linear parameter varying internal model control of open-channel systems for large operating conditions, Journal of Irrigation and Drainage Engineering, 2010, 8: 543-552
16. D.L. Yu, T.K. Chang, D.W. Yu, A stable self-learning PID control for multivariable time varying systems, Control Engineering Practice, 2007, 15: 1577-1587
17. Maciej Niedzwiecki, Michal Meller, A new approach to active noise and vibration control – Part I: The known frequency case, IEEE Trans. Signal Processing, 2009, 57(9): 3373-3386
18. Maciej Niedzwiecki, Michal Meller, A new approach to active noise and vibration control – Part II: The unknown frequency case, IEEE Trans. Signal Processing, 2010, 57(9): 3387-3398
19. F. Fahy, P. Gardonio, Sound and structural vibration (Second Edition), Academic Press Inc., 2007
20. Z. Zhang, F. Hu, H. Hua, Simulation and experiment on active vibration isolation with adaptive method. Journal of Engineering for the Maritime Environment, 2010, 224(3): 225-238
21. Z. Zhang, F. Hu, J. Wang, On saturation suppression in adaptive vibration control. Journal of Sound and Vibration, 2010, 329: 1209-1214